

Bioreducible Polymer–delivered siRNA Targeting MMP-9:

Suppression of Granulation Tissue Formation after Bare Metallic Stent Placement in a Rat Urethral Model¹

Jung-Hoon Park, RT
Jin Hyoung Kim, MD
Eun-Young Kim, PhD
Jinoo Kim, MD
Ho-Young Song, MD
Won Jong Kim, PhD
Duhwan Lee, MS
Jihong Park, RN
Soohwan Kim, RT

Purpose:

To evaluate the effectiveness of small interfering RNA (siRNA) targeting matrix metalloproteinase 9 (MMP-9) in suppressing granulation tissue formation caused by bare metallic stent placement in a rat urethral model.

Materials and Methods:

All experiments were approved by the committee of animal research. In 20 Sprague-Dawley male rats (weight range, 300–350 g), a self-expanding metallic bare stent was inserted in the urethra with fluoroscopic guidance. One group of 10 rats (group A) was treated with MMP-9 siRNA/bioreducible branched polyethylenimine–disulfide cross-linked–indocyanine green (bioreducible BPEI–SS–ICG), while the other group of 10 rats (group B) received control siRNA/bioreducible BPEI–SS–ICG treatment. All rats were sacrificed at 4 weeks. The therapeutic effectiveness of the MMP-9 siRNA/bioreducible BPEI–SS–ICG complex was assessed by comparing the two results of retrograde urethrography, histologic examination, and quantification of MMP-9 by using zymography and Western blot analysis between the two groups. The Mann-Whitney *U* test was used to evaluate differences.

Results:

Stent placement was successful in all rats without a single case of migration at follow-up. Retrograde urethrography performed 4 weeks after stent placement demonstrated significantly larger luminal diameters of the urethra within the stents in group A compared with those in group B ($P = .011$). Histologic analysis revealed that the mean percentage of granulation tissue area ($P < .001$), mean number of epithelial layers ($P < .001$), and mean thickness of submucosal fibrosis ($P < .001$) were significantly decreased in group A compared with group B. Meanwhile, the mean density of inflammatory cell infiltration did not significantly differ between the two groups ($P = .184$). Quantitative analysis disclosed MMP-9 levels to be lower in group A relative to group B, indicating positive inhibition of MMP-9 by MMP-9 siRNA/bioreducible BPEI–SS–ICG.

Conclusion:

MMP-9 siRNA/bioreducible BPEI–SS–ICG is effective for inhibiting granulation tissue formation after bare metallic stent placement in a rat urethral model.

©RSNA, 2013

¹From the Department of Radiology and Research Institute of Radiology, University of Ulsan College of Medicine, Asan Medical Center, Asanbyeongwon-gil, 388-1 Pungnap-dong, Songpa-gu, Seoul 138-736, Korea (J.H.P., J.H.K., H.Y.S., J.P., S.K.); Medical Device Development Center, Osong Medical Innovation Foundation, Chungbuk, Korea (E.Y.K.); Department of Radiology, Hanyang University Guri Hospital, Guri, Korea (J.K.); and Center for Self-assembly and Complexity, Institute for Basic Science, and Department of Chemistry, Pohang University of Science and Technology, Pohang, Korea (W.J.K., D.L.). Received April 29, 2013; revision requested June 26; final revision received September 10; accepted September 16; final version accepted September 20. Supported by the Basic Science Research Program through the National Research Foundation of Korea, funded by the Ministry of Education, Science and Technology (grant 2012R1A1A1005284). **Address correspondence to** J.H.K. (e-mail: m1fenew@daum.net).

Different types of expandable metallic stents, including bare or covered stents, have been used in the treatment of benign or malignant strictures involving nonvascular luminal organs. However, even after successful stent placement, subsequent formation of granulation tissue within the stent lumen remains a major problem and has been the center of attention, giving birth to various ongoing investigations to preserve stent patency (1–5). Therefore, it is essential to understand the pathophysiologic process of granulation tissue formation to develop ways to suppress it.

Recent research has disclosed numerous mediators involved in various steps of granulation tissue formation. Among many cytokines and growth factors that are involved in the proliferation of granulation tissue, matrix metalloproteinase 9 (MMP-9) is known to play a central role in the proliferation of fibrosis (6).

We hypothesized that, by targeting MMP-9, it is possible to prevent formation of granulation tissue after stent placement. In our study, we advocated an RNA interference (RNAi) technique, a sequence-specific gene silencing process, to target MMP-9 by using small interfering RNA (siRNA). RNAi is a mechanism of gene expression downregulation that is dependent on the target nucleotide sequence. The purpose of our study was to evaluate the effectiveness of siRNA targeting MMP-9 in suppressing granulation tissue formation caused by bare metallic stent placement in a rat urethral model.

Materials and Methods

All experimental procedures were approved by the institutional Animal Care

Advance in Knowledge

- Direct and local treatment with small interfering RNA (siRNA) targeting matrix metalloproteinase 9 (MMP-9) was effective in preventing tissue hyperplasia secondary to stent placement in a rat urethral model.

and Use Committee of Asan Medical Center (Seoul, Korea).

Animals

Our study was carried out by using rat models composed of 20 male Sprague-Dawley rats weighing 300–350 g at 9 weeks of age. Rats were maintained on a diet of rodent feed and water ad libitum at 24°C ± 1, 55% ± 10 humidity, and a 12 hour day-night cycle under specific pathogen-free conditions. Animals were acclimatized for at least 7 days prior to the start of the experiments.


Synthesis of Bioreducible Branched Polyethylenimine–Disulfide Cross-linked–Indocyanine Green

The branched polyethylenimine (BPEI)–sulfhydryl (SH) (thiolated BPEI) was synthesized by employing the previously reported method with some modifications (7). Briefly, the pH of BPEI 1.2-kDa (molecular weight of BPEI) solution was adjusted to 7.2 by adding 1N (normal concentration of ionic solution) HCl. Then, the solution was lyophilized by means of freeze-drying for 2 days to afford BPEI as a yellow solid, which was then dissolved in methanol, and the resultant solution was purged with nitrogen. After adding propylene sulfide (7 equivalent) through a syringe, the reaction mixture was stirred at 60°C for 24 hours. The product was obtained by precipitating in cold ether twice, and the degree of thiolation was measured with proton nuclear magnetic resonance spectroscopy. For the synthesis of bioreducible BPEI–disulfide cross-linked (SS), BPEI–SH was dissolved in dimethyl sulfoxide, and oxidative cross-linking was performed by stirring the solution at room temperature for 48 hours. Finally, the product was purified by using dialysis against deionized

water (molecular weight cutoff, 8000) and lyophilized.

Indocyanine green (ICG) is a fluorescent dye, and it is deemed suitable in *in vivo* studies, as it emits near-infrared fluorescence, and unlike normal fluorescence, it provides deep tissue penetration. ICG dye was conjugated to bioreducible BPEI–SS according to the reported method with some modifications (8). Triethylamine and 6-aminohexanoic acid were added to a solution of ICG in anhydrous dimethylformamide and stirred for 5 hours at 85°C. The product was purified with column chromatography by using ethylacetate and methanol as eluent (AcOEt/MeOH, 70/30–0/100) to afford the compound as a blue solid (ICG–COOH). To synthesize bioreducible BPEI–SS–ICG, *N*-(3-dimethylaminopropyl)-*N'*-ethylcarbodiimide hydrochloride) was added to the ICG–COOH in anhydrous dimethylformamide at room temperature. Then, a solution of bioreducible BPEI–SS in dimethylformamide was added, and the reaction mixture was stirred at room temperature for 24 hours. The product was purified by means of repeated ultrafiltration against methanol and water (molecular weight cutoff, 10000) twice, followed by lyophilization. The degree of ICG conjugation with bioreducible BPEI–SS was

Published online before print

10.1148/radiol.13130980 Content code: 

Radiology 2014; 271:87–95

Abbreviations:

BPEI = branched polyethylenimine
ICG = indocyanine green
MMP-9 = matrix metalloproteinase 9
RNAi = RNA interference
siRNA = small interfering RNA
SS = disulfide cross-linked

Author contributions:

Guarantors of integrity of entire study, J.H.K., H.Y.S.; study concepts/study design or data acquisition or data analysis/interpretation, all authors; manuscript drafting or manuscript revision for important intellectual content, all authors; approval of final version of submitted manuscript, all authors; literature research, J.H.P., J.H.K., E.Y.K., J.K., H.Y.S., W.J.K., J.P., S.K.; clinical studies, J.K., H.Y.S.; experimental studies, J.H.P., J.H.K., E.Y.K., D.L., J.P., S.K.; statistical analysis, J.H.P., J.H.K., E.Y.K.; and manuscript editing, J.H.P., J.H.K., E.Y.K., J.K., H.Y.S., W.J.K.

Conflicts of interest are listed at the end of this article.

Implication for Patient Care

- Local therapy by using bioreducible branched polyethylenimine – disulfide cross-linked–indocyanine green–delivered siRNA targeting MMP-9 could be used as a newer approach for preventing stent-related tissue hyperplasia.

estimated by using the ultraviolet and visible spectrometry method. Bioreducible BPEI-SS-ICG can form nano-sized complex (polyplex) with siRNA by means of electrostatic interaction. Once polyplex gets internalized into the cell, it can escape from the endosome through the proton-sponge effect. Furthermore, due to the reducing environment of cytosolic compartments, the disulfide bond can be reduced and cleaved to the thiol group. As a result, cross-linked bioreducible BPEI can be degraded to low-molecular-weight BPEI.

Preparation of siRNA/bioreducible BPEI-SS-ICG

siRNA targeting rat MMP-9 and control siRNA (nonspecific siRNA) were purchased from a commercial supplier (Qiagen Technologies, Coralville, Iowa). The MMP-9-silencing effect of siRNAs was determined by using gelatin zymography and Western blot analysis. Complexes were formed by gently mixing siRNA with bioreducible BPEI-SS-ICG (in 5% glucose) solutions. The siRNA/bioreducible BPEI-SS-ICG complex formation was confirmed by polyacrylamide gel retardation assays. The bioreducible BPEI-SS-ICG and the siRNA dose of 60 $\mu\text{mol/L}$ complex (30:1 nitrogen-phosphorus ratios) were used in the animal study.

Stent Construction and Placement

The self-expandable metallic bare stent was woven from a single thread of nitinol wire filament of 0.1 mm in thickness (Taewoong, Kimpo, Gyunggi, Korea). Its diameter and length were 3 mm and 8 mm, respectively, at full expansion. The stent size was chosen considering the diameter (2.8 mm) and length (15 mm) of the normal urethra in rats weighing 300–350 g at 9 weeks of age (9). It possessed six bend points on each end with radiopaque markers on either end to aid accurate deployment within the urethra (Fig 1).

Details in regard to the stent placement technique have been described by researchers in previous studies (9).

Techniques in Complex Treatment

The rats were randomized and divided into two groups of 10, where the first

group, group A (treatment group), was treated with MMP-9 siRNA/bioreducible BPEI-SS-ICG complex after placement of the urethral stent, while the second group, group B (control group), received control siRNA/bioreducible BPEI-SS-ICG complex treatment following stent placement (E.Y.K. and J.H.P., with more than 5 years of experience in interventional radiology). In both groups, siRNA/bioreducible BPEI-SS-ICG complex was administered retrograde via the urethral opening on a weekly basis for 3 weeks. To retain the treatment complex within the urethra, its spillage into the bladder was prevented by clamping the bladder neck with a clamp (Jeungdo Bio & Plant, Seoul, Korea). This was achieved by performing an open midline incision in the lower abdominal wall, with the animal anesthetized, and partially extracting the bladder for accurate visualization and placement of the device. For the same purpose, a second clamp was applied to the penile urethra to obstruct outflow. Both clamps were maintained for 30 minutes before they were removed. Repair of the abdominal wall was performed thereafter. The rats were maintained in a temperature-controlled room (24°C) and supplied with autoclaved food and water during the recovery period. On the 4th week, all rats in group A and group B were sacrificed to evaluate the degree of stent-induced tissue hyperplasia in each group.

The properties of the capability of bioreducible BPEI-SS-ICG to deliver MMP-9 siRNA or control siRNA in vivo were assessed in all rats after 1 minute and 30 minutes after injection of the MMP-9 siRNA/bioreducible BPEI-SS-ICG or control siRNA/bioreducible BPEI-SS-ICG by using an imaging system (Vivo Vision Systems, IVIS 200 Series Imaging System; Xenogen, Alameda, Calif). ICG absorbed mainly between 600 nm and 900 nm and emitted fluorescence between 750 nm and 950 nm. During imaging, rats were anesthetized with 2.5% isoflurane gas in the oxygen flow (1.5 L/min). Images were analyzed by using software (Living Image 2.50-Igor Pro 4.09;

Figure 1



Figure 1: Self-expanding bare metallic stent. When fully expanded, the stent is 3 mm in diameter and 8 mm in length. Gold markers were attached to either end of the stent.

Xenogen), according to the manufacturer's instructions.

Urethrographic Examination

Fluoroscopically guided (Artis Zee Multipurpose; Siemens, Muenchen, Germany) retrograde urethrography was performed in right anterior oblique projections with use of a calibrated catheter, with anesthesia, in all rats immediately after stent placement to verify position of the stent and passage of contrast medium (Omnipaque 300; GE Healthcare, Cork, Ireland). This procedure was repeated 4 weeks later to assess changes in diameter within the stent. Luminal diameter was measured on urethrograms, and a calibrated catheter, which was constructed in our research laboratory, was used for reference. A software package (Photoshop, version 6.0; Adobe Systems, Palo Alto, Calif) was used to acquire digital measurements of the inner luminal diameter of the segment with the stent at three different levels. Measurements were repeated three times at each level, yielding the average value per level, and these values were subsequently averaged to obtain an overall average diameter of the segment of the urethra with the stent. Urethral stenosis secondary to granulation tissue formation within the stents was graded according to severity with reference to a previous article (9), as follows: grade 0, normal; grade 1, mild urethral wall irregularity; grade 2, filling defect of less than one-half of the stent diameter; and grade 3, filling defect of more than one-half of the stent diameter. Grading of urethral

stenosis was performed by three observers (J.H.K., E.Y.K., and J.H.P., with more than 5 years of experience in interventional radiology) in consensus.

Histologic Examination

All rats were sacrificed by means of administration of inhalable pure carbon dioxide. Surgical exploration of the urethra and urinary bladder were performed. The urethral tissue samples were fixed in 10% neutral buffered formalin for 24 hours. Fixed tissue samples were then sectioned transversely at the proximal, middle, and distal portions of the segment with the stent. Cut stent wires were removed from the specimens, and care was taken to preserve the hyperplastic tissue area. The specimens were then processed for microscopic examination. Histologic evaluation was performed with a microscope to determine the percentage of granulation tissue–related stenosis calculated with $100 \cdot (1 - [L_{\text{sten}}/L_{\text{orig}}])$, where L_{sten} is stenotic lumen cross-sectional area and L_{orig} is original lumen cross-sectional area. The degree of submucosal inflammatory cell infiltration (macrophage, monocyte, lymphocyte) was subjectively determined according to the distribution and density of the inflammatory cells (grade 1, mild; grade 2, mild to moderate; grade 3, moderate; grade 4, moderate to severe; and grade 5, severe) (10). The average values for the number of epithelial layers and thickness of submucosal fibrosis were obtained from averaging eight points (including maximum and minimum points) around the circumference. One pathologist (J.Y.R., with 30 years of experience in genitourinary pathology) carried out urethral diameter measurements at three different levels for each animal in a manner similar to that described above for diameter measurements on retrograde urethrograms. The average value per level and overall average diameter were yielded through this process. Histologic analysis of the urethra was performed with a microscope (BX51; Olympus, Tokyo, Japan) equipped with magnification capabilities of $\times 1.25$, $\times 20$, and $\times 40$. Measurements were obtained by

using software (Image-Pro Plus; Media Cybernetics, Silver Spring, Md).

Quantitative Analysis for MMP-9

MMP-9 in the rat urethral tissue was quantified by means of zymography and Western blot analysis. For quantification of MMP-9, the tissue was snap-frozen in liquid nitrogen and stored at -196°C in a nitrogen tank until extraction of protein.

Gelatin zymography.—The samples were prepared with homogenization of the tissues in the lysis buffer (Cell Signaling Technology, Beverly, Mass). The homogenates were centrifuged at $10000g$ for 15 minutes at 4°C , and the supernatants were collected for analysis. Tissue extracts were analyzed by using 10% sodium dodecylsulfate–polyacrylamide gel electrophoresis (SDS-PAGE; Invitrogen, Grand Island, NY) with 0.1% gelatin incorporated as a substrate for gelatinolytic proteases with nonreducing conditions at 125 V for 90 minutes. Equal amounts of tissue extract protein (20 μg), determined by using the method of Bradford (11), were loaded onto the gels. After electrophoresis, the gels were incubated twice in renaturing buffer (2.5% TritonX-100; Sigma Chemical, St Louis, Mo) for 30 minutes at room temperature, with gentle agitation to remove sodium dodecylsulfate. The gels were equilibrated once for 30 minutes at room temperature in developing buffer (50 mmol/L tris[hydroxymethyl]amino-methane [Tris; Sigma Chemical] base, 50 mmol/L Tris HCl [Sigma Chemical], 0.2 mol/L NaCl, 5 mmol/L CaCl_2 , 0.02% Brij 35 [Sigma Chemical]), and then the membranes were incubated at 37°C overnight in fresh developing buffer to activate metalloproteinases. The gels were stained with 0.5% Coomassie brilliant blue R-250 (Bio-Rad, Hercules, Calif) for 2 hours and destained in a destaining solution of methanol, acetic acid, and distilled water in a ratio of 4.5:1:4.5. The molecular weight of each band was estimated by comparison with the positions of known molecular-weight standards (Bio-Rad).

Western blot analysis.—Equal amounts of protein (30 μg) were

resolved with 10% sodium dodecylsulfate–polyacrylamide gel electrophoresis. Gels containing proteins were transferred to the nitrocellulose membranes, and the membranes were blocked with 5% nonfat skim milk dissolved in Tris buffer saline containing 0.1% Tween 20 (Sigma Chemical) for 1 hour. After membrane washing with Tris buffer saline containing 0.1% Tween 20 for three times, membranes were incubated in primary antibodies diluted in Tris-buffered saline containing 0.1% Tween 20 at 4°C overnight with gentle agitation and again the membranes were washed. Then, they were incubated in secondary antibodies conjugated to horseradish peroxidase. The target proteins were detected by using reagents (ECL Western Blotting Detection Reagents; Amersham Biosciences, Little Chalfont, Buckinghamshire, England). Targets were MMP-9 primary antibodies (Abcam, Cambridge, Mass) and β -actin primary antibodies (Sigma Chemical).

Statistical Analysis

Differences between animal groups with respect to the degree of urethral narrowing demonstrated at retrograde urethrography, percentage of granulation tissue formation, values for the number of epithelial layers, thickness of submucosal fibrosis, and the extent of inflammation demonstrated on microscopic images were tested by using the Mann-Whitney U test. A P value of less than .05 was considered to indicate a significant difference. Statistical software (SPSS, version 19.0; SPSS, Chicago, Ill) was used to perform the analyses.

Results

Stent Placement

Stent placement was technically successful, without difficulty, in all rats. A small amount of hematuria occurred immediately after stent placement in all rats, but it spontaneously subsided. During stent placement in two rats in group B, the stent introducer was responsible for urethral perforation.

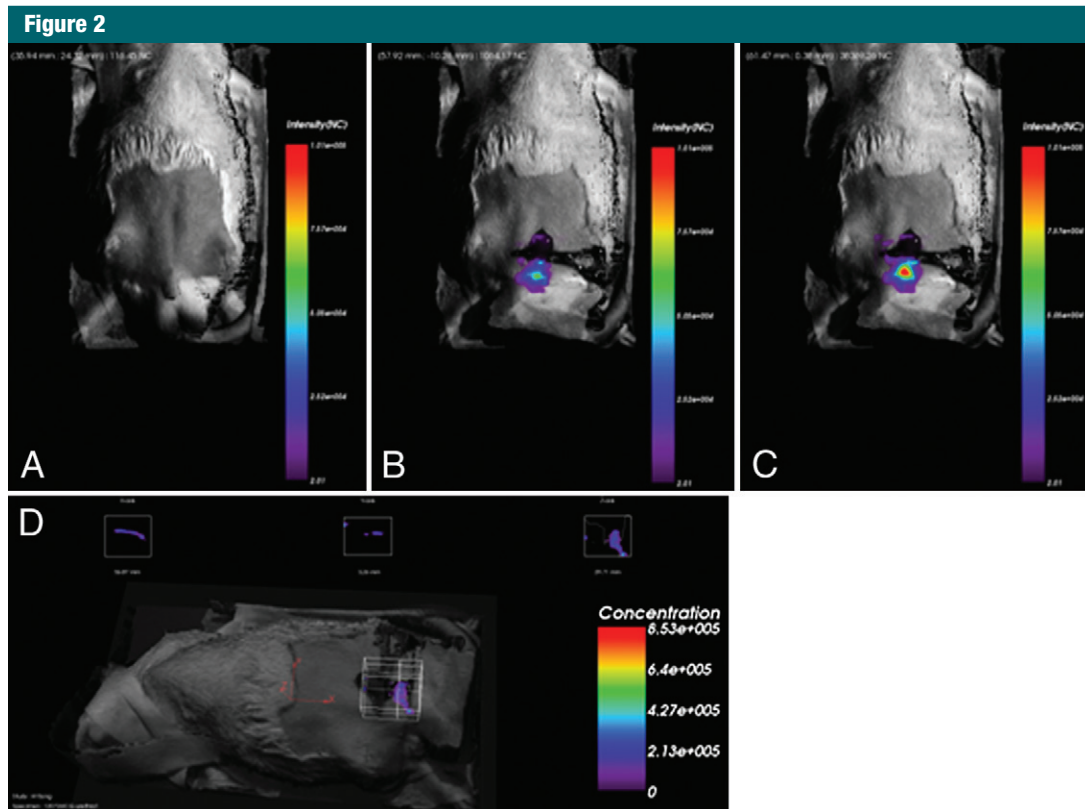


Figure 2: In vivo imaging in a rat with 2 mg/mL penis injection of MMP-9 siRNA/bioreducible BPEI-SS-ICG. *A*, Before injection. *B*, At 1 minute after injection. *C*, At 30 minutes after injection. *D*, Image is a three-dimensional reconstruction of rat body and organs of interest. Color bar = signal efficiency of the fluorescence emission coming out from the animal.

However, spontaneous healing of urethral perforation was demonstrated at retrograde urethrography performed 4 weeks after the event. All rats survived until the end of the study without a single case of stent migration.

Optical Imaging in Vivo

Figure 2 shows the optical images of a rat before (Fig 2, *A*) and after 1 minute (Fig 2, *B*) and 30 minutes from the injection of MMP-9 siRNA/bioreducible BPEI-SS-ICG (Fig 2, *C*). Figure 2, *D*, shows the three-dimensional reconstruction of the rat body and the organs of interest. Also, in this case, after the injection of the MMP-9 siRNA/bioreducible BPEI-SS-ICG, optical images showed signal intensity enhancement in the region corresponding to the urethra. All rats in both groups showed positive signal intensity enhancement after 30 minutes from the injection of MMP-9 siRNA/bioreducible

BPEI-SS-ICG or control siRNA/bioreducible BPEI-SS-ICG.

Urethrographic Results

The average luminal diameter of the urethra within the proximal, middle, and distal segments of the stent and average overall luminal diameter at follow-up retrograde urethrography for groups A and B are summarized in Table 1. In group A, the mean luminal diameter of the three segments at follow-up retrograde urethrography was significantly larger compared with that in group B at 4 weeks after stent placement (2.32 ± 0.45 vs 1.78 ± 0.31 , $P < .001$) (Fig 3). When data from the two rats with urethral perforation were omitted, these results retained significance (mean, 2.32 ± 0.45 vs 1.86 ± 0.38 ; $P < .001$). The grades of granulation tissue formation after stent placement in group A were determined to be grade 1 in seven rats and grade 2 in

the remaining three rats. In group B, granulation grades were determined to be grade 1 in two rats, grade 2 in three rats, and grade 3 in the remaining five rats.

Histologic Results

The histologic findings are summarized in Table 2, and an example is shown in Figure 4. Granulation tissue formation was seen in both groups, but in correlation with the findings at retrograde urethrography, the mean percentage of granulation tissue area was lower for group A compared with group B (62.38 ± 11.20 vs 70.22 ± 7.17 , $P = .011$), indicating effective suppression of stent-induced tissue hyperplasia with MMP-9 siRNA/bioreducible BPEI-SS-ICG. Furthermore, the mean number of epithelial layers and mean thickness of submucosal fibrosis in millimeters were significantly decreased in group A relative to group B, with 3.42 ± 0.78

Table 1

Urethrographic Findings after Stent Placement

Location	Group A (n = 10)	Group B (n = 10)	Group B (n = 8)*	P Value, Group A Versus B	P Value, Group A Versus B*
Proximal	2.48 ± 0.42	1.79 ± 0.18	1.83 ± 0.16	<.001	<.001
Middle	2.27 ± 0.45	1.78 ± 0.23	1.84 ± 0.22	.01	.024
Distal	2.22 ± 0.48	1.78 ± 0.47	1.89 ± 0.48	.063	.181
Average	2.32 ± 0.45	1.78 ± 0.31	1.86 ± 0.38	<.001	<.001

Note.—Data are mean diameters of the area with a stent in millimeters ± standard deviations except where otherwise indicated; diameters and *P* values were determined at 4 weeks after stent placement.

* For group B, data from two rats with urethral perforation were omitted.

Figure 3

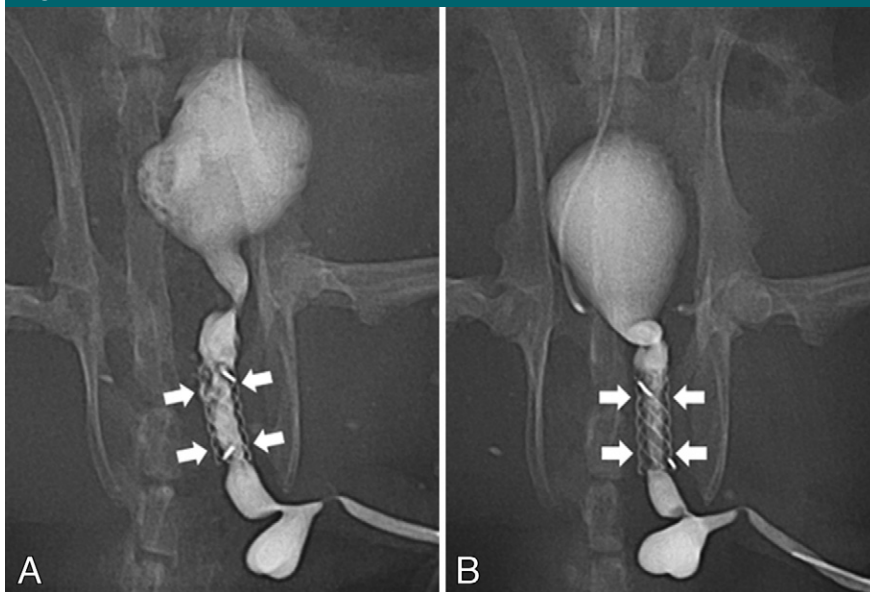


Figure 3: Retrograde urethrogram performed 4 weeks following stent placement in, *A*, group A animal (treatment group) and, *B*, group B animal (control group) demonstrates a larger luminal diameter (arrows) in group A animal relative to group B animal owing to suppressed stent-induced tissue hyperplasia with MMP-9 siRNA/bioreducible BPEI-SS-ICG.

versus 5.90 ± 1.01 ($P < .001$) and 0.75 ± 0.17 versus 1.48 ± 0.39 ($P < .001$), respectively. The mean density grade of inflammatory cell infiltration did not differ among the two groups, with 2.50 ± 0.72 versus 2.71 ± 0.81 ($P = .184$). When data from the two rats with urethral perforation were omitted, these results also retained significance (Table 3).

Quantitative Analysis for MMP-9

The identities of the lytic zones on the gelatin zymograms represented MMP-9

(92 kDa). The 10% sodium dodecylsulfate-polyacrylamide gel electrophoresis zymography and Western blot analyses revealed that MMP-9 expression was more substantially inhibited in group A than in group B (Figs 5, 6). These results indicated effective gene silencing with siRNA targeting MMP-9.

Discussion

Recent advances in stent technology have greatly contributed to increased success rates in stent placement in

various obstructive conditions of the hollow viscera. The gastrointestinal and biliary tracts, which are susceptible to both benign and malignant strictures, have largely benefited from such developments. With recent achievements with respect to technical success in stent placement, attention has now turned to long-term preservation of stent patency (3,12–15). This direction has resulted in new ideas to preserve stent patency, leading to the development of covered stents and drug-eluting stents among others (4,16–19). While the former creates a physical barrier to hinder ingrowth of benign tissue hyperplasia and malignant tissue, the latter focuses on prevention of their growth. With regard to prevention of benign tissue hyperplasia that is often a cause of stent obstruction induced by the stent itself, various substances, such as the ALK-5 inhibitor 3-{[4-(6-methylpyridin-2-yl)-5-(quinolin-6-yl)-1H-imidazol-2-yl] methyl} benzamide (IN-1233), dexamethasone, paclitaxel, and proteinase inhibitors, have been applied in vitro and in vivo in an effort to discover one that provides optimal suppression of granulation tissue formation (9,10,14,15,19–23). As past research has shown, granulation tissue is a result of tissue remodeling, which itself is a complex multistep process involving a variety of mediators.

Matrix metalloproteinases, a family of zinc-dependent proteinases with extracellular matrix remodeling and degrading properties, are among those that have been demonstrated to play a key role in the process of tissue remodeling (6,24,25). MMP-9 is one of the two matrix metalloproteinases that has been found to be highly expressed during the process of vascular remodeling and tumor growth. Along the same line, Shin et al (15) reported that expression of MMP-9 was significantly increased in tracheal granulation tissue formation induced by stent placement relative to levels found in normal tissue in a rat tracheal model. On the basis of these results, inhibition of tissue hyperplasia by targeting MMP-9 could potentially halt the process of stent-induced tissue growth. Matrix metalloproteinase

Table 2

Histologic Findings after Stent Placement in Rat Urethra

Location	Percentage of Granulation Tissue Area		No. of Epithelial Layers		Thickness of Submucosal Fibrosis (mm)		Inflammatory Cell Infiltration					
	Group A	Group B	P Value	Group A	Group B	P Value	Group A	Group B	P Value			
Proximal	59.80 ± 10.96	72.66 ± 9.77	.028	3.33 ± 0.68	5.69 ± 1.18	<.001	0.78 ± 0.20	1.75 ± 0.36	<.001	2.27 ± 0.75	2.30 ± 0.75	.964
Middle	63.88 ± 10.32	73.12 ± 10.59	.013	3.38 ± 0.78	5.93 ± 0.96	<.001	0.72 ± 0.14	1.39 ± 0.42	<.001	2.55 ± 0.70	2.93 ± 0.79	.159
Distal	62.28 ± 13.68	65.50 ± 11.34	.770	3.56 ± 0.89	6.07 ± 0.09	<.001	0.76 ± 0.18	1.32 ± 0.21	<.001	2.68 ± 0.70	2.85 ± 0.77	.543
Average	62.38 ± 11.20	70.22 ± 7.17	.011	3.42 ± 0.78	5.90 ± 1.01	<.001	0.75 ± 0.17	1.48 ± 0.39	<.001	2.50 ± 0.72	2.71 ± 0.81	.184

Note.—Each group consisted of 10 animals. Data are means ± standard deviations except where otherwise indicated

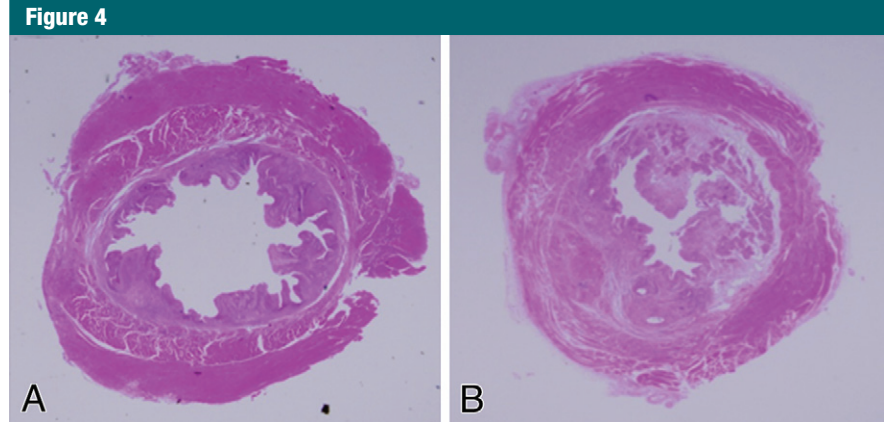


Figure 4: Histologic specimens of, *A*, group A animal (treatment group) and, *B*, group B animal (control group) revealed granulation tissue formation in both groups, but the average area of granulation tissue was lower for group A relative to group B, indicating effective suppression of stent-induced tissue hyperplasia with MMP-9 siRNA/bioreducible BPEI-SS-ICG. (Hematoxylin-eosin; original magnification, ×1.25.)

inhibitors that have been developed and applied in medicine include GM6001, TIMP, and doxycycline, all of which have demonstrated therapeutic effect to some extent (26–28). However, concerns about their safety, such as drug toxicity and nonspecific effects, have hindered their widespread use.

In our study, we advocated the RNAi technique by using bioreducible BPEI-SS-ICG–delivered siRNA to suppress granulation tissue formation within the stent lumen. Ever since its introduction 10 years ago, the phenomenon of RNAi has drawn widespread attention of researchers from all over the world (29). It is an RNA-dependent gene-silencing process controlled by the RNA-induced silencing complex, or RISC, that moderates the activity of genes in living organisms. Theoretically, RNAi can be exploited in therapeutic medicine by introducing siRNA into specific target genes. However, previous attempts at delivery of siRNA into cells for gene silencing have gone through trials and errors owing to the lack of efficient delivery systems. Stability of the siRNA after its administration into the body and efficient cellular uptake and transfection are key steps to the successful delivery of siRNA into the target tissue. In this light, the selection of an appropriate delivery system (vector) is mandatory, and, recently, a majority of proposed clinical applications of RNAi

use siRNA duplexes, delivered into cells by nonviral vectors. Among numerous nonviral vectors that have been applied, bioreducible BPEI is regarded as one of the most effective nonviral vectors (30). In the current study, we chose bioreducible BPEI-SS-ICG for the delivery system of siRNA to target MMP-9. Even with difficulties that lie in its application, RNAi offers an alternative access to disease therapy where it prevents the expression of disease-associated proteins at the RNA level, in contrast to most drugs that act at the protein level.

At comparison of the results of retrograde urethrography between group A and group B, the luminal diameter of the urethra with a stent was larger for the former, indicating effective suppression of tissue hyperplasia following stent insertion. To support the gross findings at urethrography, histologic examination of the urethra was performed to reveal a lower area of granulation tissue in group A, thereby positively correlating with the urethrographic results. In our study, urethral perforation caused by the stent introducer during stent placement occurred in two rats in group B. However, when data from the two rats with urethral perforation were omitted, significant results were retained. In the study by Shin et al (15), zymography and Western blot analysis targeting MMP-9 demonstrated overexpressed MMP-9 in the

Table 3

Histologic Findings When Data from Two Rats with Urethral Perforation in Group B Were Omitted

Location	Percentage of Granulation Tissue Area		No. of Epithelial Layers		Thickness of Submucosal Fibrosis (mm)		Inflammatory Cell Infiltration				
	Group A	Group B	Group A	Group B	Group A	Group B	Group A	Group B			
Proximal	59.80 ± 10.96	70.73 ± 10.29	.05	3.33 ± 0.68	5.61 ± 1.21	<.001	0.78 ± 0.20	1.59 ± 0.52	2.27 ± 0.75	2.25 ± 0.51	.814
Middle	63.88 ± 10.32	71.54 ± 11.15	.165	3.38 ± 0.78	5.91 ± 0.98	<.001	0.72 ± 0.14	1.28 ± 0.19	2.55 ± 0.70	2.91 ± 0.82	.092
Distal	62.28 ± 13.68	63.42 ± 11.67	.902	3.56 ± 0.89	5.96 ± 0.28	<.001	0.76 ± 0.18	1.31 ± 0.21	2.68 ± 0.70	2.71 ± 0.72	.796
Average	62.38 ± 11.20	68.56 ± 11.20	.048	3.42 ± 0.78	5.84 ± 1.11	<.001	0.75 ± 0.17	1.39 ± 0.43	2.50 ± 0.72	2.68 ± 0.69	.267

Note.—Group A consisted of 10 animals and group B consisted of eight animals. Data are means ± standard deviations except where otherwise indicated.

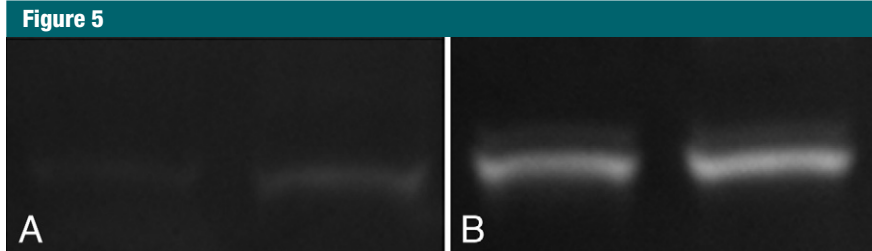


Figure 5: The 10% sodium dodecylsulfate–polyacrylamide gel electrophoresis zymography revealed that MMP-9 expression was inhibited in, A, group A relative to, B, group B, indicating effective gene silencing with siRNA targeting MMP-9.



Figure 6: Western blot analysis revealed that MMP-9 expression was inhibited in, A, group A relative to, B, group B, indicating effective gene silencing with siRNA targeting MMP-9.

stent-induced granulation tissue formation but not in the normal tissue in a rat tracheal model. They suggested that MMP-9 may be a key prognostic factor in stent-induced granulation tissue formation and that tailored treatment targeting MMP-9 could be promising to control granulation tissue formation. The findings in the present study are in line with theirs in which its intent was to suppress MMP-9 by using the RNAi technique. The results acquired from this study were positive where MMP-9 siRNA successfully inhibited MMP-9 expression, not only shown by suppressed tissue growth within the stents but also demonstrated at quantitative analysis of MMP-9 with zymography and Western blot analyses.

There were a few limitations to our study. The first limitation lies in the dose of MMP-9 siRNA/bioreducible

BPEI-SS-ICG and treatment schedule. Only a single fixed dose was given to each rat, yielding the results in our study. However, the optimal dose for suppressing tissue hyperplasia is not known, and we cannot exclude the possibility that the results would be affected by treatment dose. Second, although we chose to use rats treated with control siRNA/bioreducible BPEI-SS-ICG as the animal model control, the strength of the results may be enhanced by using MMP-9 knockout animals instead. According to the theory on which our study is based, tissue hyperplasia would neither be induced nor suppressed in MMP-9 knockout animals. Third, results of MMP-9 siRNA/bioreducible BPEI-SS-ICG withdrawal were not obtained. If it had been shown that tissue hyperplasia was reinduced after withdrawal of treatment, it would

have provided further evidence to support the effectiveness of MMP-9 siRNA/bioreducible BPEI-SS-ICG in inhibiting stent-induced tissue hyperplasia. Fourth, the side effects of MMP-9-targeting siRNA were not evaluated in our study. Given that nonspecific effects of RNAi treatment drugs are huge drawbacks to their application in medicine, further research should be undertaken to clarify the issue.

In conclusion, MMP-9 siRNA/bioreducible BPEI-SS-ICG is effective for inhibiting granulation tissue formation after bare metallic stent placement in a rat urethral model.

Disclosures of Conflicts of Interest: J.H.P. No relevant conflicts of interest to disclose. J.H.K. No relevant conflicts of interest to disclose. E.Y.K. No relevant conflicts of interest to disclose. J.K. No relevant conflicts of interest to disclose. H.Y.S. No relevant conflicts of interest to disclose. W.J.K. No relevant conflicts of interest to disclose. D.L. No relevant conflicts of interest to disclose. J.P. No relevant conflicts of interest to disclose. S.K. No relevant conflicts of interest to disclose.

References

- Song HY, Park H, Suh TS, et al. Recurrent traumatic urethral strictures near the external sphincter: treatment with a covered, retrievable, expandable nitinol stent—initial results. *Radiology* 2003;226(2):433–440.
- Holm AN, de la Mora Levy JG, Gostout CJ, Topazian MD, Baron TH. Self-expanding plastic stents in treatment of benign esophageal conditions. *Gastrointest Endosc* 2008;67(1):20–25.
- Kim JH, Shin JH, Song HY, Shim TS, Yoon CJ, Ko GY. Benign tracheobronchial strictures: long-term results and factors affecting airway patency after temporary stent placement. *AJR Am J Roentgenol* 2007;188(4):1033–1038.
- Song HY, Shin JH, Yoon CJ, et al. A dual expandable nitinol stent: experience in 102 patients with malignant gastroduodenal strictures. *J Vasc Interv Radiol* 2004;15(12):1443–1449.
- Song HY, Lee DH, Seo TS, et al. Retrievable covered nitinol stents: experiences in 108 patients with malignant esophageal strictures. *J Vasc Interv Radiol* 2002;13(3):285–293.
- Galis ZS, Khatir JJ. Matrix metalloproteinases in vascular remodeling and atherogenesis: the good, the bad, and the ugly. *Circ Res* 2002;90(3):251–262.
- Son S, Singha K, Kim WJ. Bioreducible BPEI-SS-PEG-cNGR polymer as a tumor targeted nonviral gene carrier. *Biomaterials* 2010;31(24):6344–6354.
- Masotti A, Vicennati P, Boschi F, Calderan L, Sbarbati A, Ortaggi G. A novel near-infrared indocyanine dye-polyethylenimine conjugate allows DNA delivery imaging in vivo. *Bioconjug Chem* 2008;19(5):983–987.
- Kim JH, Song HY, Park JH, Yoon HJ, Park HG, Kim DK. IN-1233, an ALK-5 inhibitor: prevention of granulation tissue formation after bare metallic stent placement in a rat urethral model. *Radiology* 2010;255(1):75–82.
- Shin JH, Song HY, Choi CG, et al. Tissue hyperplasia: influence of a paclitaxel-eluting covered stent—preliminary study in a canine urethral model. *Radiology* 2005;234(2):438–444.
- Bradford MM. A rapid and sensitive method for the quantitation of microgram quantities of protein utilizing the principle of protein-dye binding. *Anal Biochem* 1976;72(1-2):248–254.
- Li YD, Song HY, Kim JH, et al. Evaluation of formation of granulation tissue caused by metallic stent placement in a rat urethral model. *J Vasc Interv Radiol* 2010;21(12):1884–1890.
- Mayoral W, Fleischer D, Salcedo J, Roy P, Al-Kawas F, Benjamin S. Nonmalignant obstruction is a common problem with metal stents in the treatment of esophageal cancer. *Gastrointest Endosc* 2000;51(5):556–559.
- Kim EY, Shin JH, Jung YY, Shin DH, Song HY. A rat esophageal model to investigate stent-induced tissue hyperplasia. *J Vasc Interv Radiol* 2010;21(8):1287–1291.
- Shin JH, Sung KB, Kim EY, Shin DH, Song HY. A rat tracheal model to investigate stent-induced tissue hyperplasia: a pilot study. *J Vasc Interv Radiol* 2010;21(12):1878–1883.
- Lopera JE, Alvarez O, Castaño R, Castañeda-Zuñiga W. Initial experience with Song's covered duodenal stent in the treatment of malignant gastroduodenal obstruction. *J Vasc Interv Radiol* 2001;12(11):1297–1303.
- Jung GS, Song HY, Seo TS, et al. Malignant gastric outlet obstructions: treatment by means of coaxial placement of uncovered and covered expandable nitinol stents. *J Vasc Interv Radiol* 2002;13(3):275–283.
- Park SJ, Shim WH, Ho DS, et al. A paclitaxel-eluting stent for the prevention of coronary restenosis. *N Engl J Med* 2003;348(16):1537–1545.
- Strecker EP, Gabelmann A, Boos I, et al. Effect on intimal hyperplasia of dexamethasone released from coated metal stents compared with non-coated stents in canine femoral arteries. *Cardiovasc Intervent Radiol* 1998;21(6):487–496.
- Nakagawa H, Shuto K, Isaji M, Watanabe K, Tsurufuji S. Proteinase inhibitors suppress the formation of granulation tissue in the carrageenin-induced inflammation in rats. *J Pharmacobiodyn* 1981;4(6):429–435.
- Shin JH, Song HY, Seo TS, et al. Influence of a dexamethasone-eluting covered stent on tissue reaction: an experimental study in a canine bronchial model. *Eur Radiol* 2005;15(6):1241–1249.
- Rechavia E, Litvack F, Fishbien MC, Nakamura M, Eigler N. Biocompatibility of polyurethane-coated stents: tissue and vascular aspects. *Cathet Cardiovasc Diagn* 1998;45(2):202–207.
- Shlomi D, Peled N, Shitrit D, Bendayan D, Amital A, Kramer MR. Protective effect of immunosuppression on granulation tissue formation in metallic airway stents. *Laryngoscope* 2008;118(8):1383–1388.
- Nagase H, Woessner JF Jr. Matrix metalloproteinases. *J Biol Chem* 1999;274(31):21491–21494.
- Vu TH, Werb Z. Matrix metalloproteinases: effectors of development and normal physiology. *Genes Dev* 2000;14(17):2123–2133.
- Martin-Martin B, Tovell V, Dahlmann-Noor AH, Khaw PT, Bailly M. The effect of MMP inhibitor GM6001 on early fibroblast-mediated collagen matrix contraction is correlated to a decrease in cell protrusive activity. *Eur J Cell Biol* 2011;90(1):26–36.
- Nagase H, Visse R, Murphy G. Structure and function of matrix metalloproteinases and TIMPs. *Cardiovasc Res* 2006;69(3):562–573.
- Smith GN Jr, Mickler EA, Hasty KA, Brandt KD. Specificity of inhibition of matrix metalloproteinase activity by doxycycline: relationship to structure of the enzyme. *Arthritis Rheum* 1999;42(6):1140–1146.
- Fire A, Xu S, Montgomery MK, Kostas SA, Driver SE, Mello CC. Potent and specific genetic interference by double-stranded RNA in *Caenorhabditis elegans*. *Nature* 1998;391(6669):806–811.
- Deng R, Yue Y, Jin F, et al. Revisit the complexation of PEI and DNA - how to make low cytotoxic and highly efficient PEI gene transfection non-viral vectors with a controllable chain length and structure? *J Control Release* 2009;140(1):40–46.